Chiral Honeycomb Lattices of Non-planar π-conjugated Supramolecules with Protected Dirac and Flat Bands

Ryohei Nemoto[1], Ryuichi Arafune[1], Saya Nakano[2], Masahisa Tsuchiizu[2], Noriaki Takagi[3], Rie Suizu[4,5]*, Takashi Uchihashi[1,6]**, and Kunio Awaga[4]***

[1] Research Center for Materials Nanoarchitectonics (MANA), National Institute for Materials Science, 1-1, Namiki, Tsukuba, Ibaraki 305-0044, Japan

[2] Department of Physics, Nara Women's University, Kitauoyanishi-machi, Nara 630-8506, Japan

[3] Graduate School of Human and Environmental Studies, Kyoto University, Yoshida-nihonmatsu-cho, Sakyo-ku, Kyoto 606-8501, Japan

[4] Department of Chemistry and IRCCS, Nagoya University, Furo-cho, Chikusa-ku, Nagoya 464-8602, Japan.

[5] Japan Science and Technology Agency (JST), PRESTO, 4-1-8 Honcho, Kawaguchi, Saitama, 332-0012, Japan

[6] Graduate School of Science, Hokkaido University, Kita-10 Nishi-8, Kita-ku, Sapporo 060-0810, Japan

*email: suizu@chem.nagoya-u.ac.jp

** email: UCHIHASHI.Takashi@nims.go.jp

***email: awaga.kunio.h8@f.mail.nagoya-u.ac.jp

ABSTRACT

The honeycomb lattice is a fundamental two-dimensional (2D) network that gives rise to surprisingly rich electronic properties. While its expansion to 2D supramolecular assembly is conceptually appealing, its realization is not straightforward because of weak intermolecular coupling and strong influence of a supporting substrate. Here we show that the application of a triptycene derivative with phenazine moieties, Trip-Phz, solves this problem due to its strong intermolecular π-π pancake bonding and non-planar geometry. Our scanning tunneling microscopy (STM) measurements demonstrate that Trip-Phz molecules self-assemble on a Ag(111) surface to form chiral and commensurate honeycomb lattices. Electronically, the network can be viewed as a hybrid of honeycomb and kagome lattices. The Dirac and flat bands predicted by a simple tight-binding model are reproduced by total density functional theory (DFT) calculations, highlighting the protection of the molecular bands from the Ag(111) substrate. The present work offers a rational route for creating chiral 2D supramolecules that can accommodate pristine Dirac and flat bands simultaneously.

KEYWORDS

Honeycomb lattice, Kagome lattice, self assembly, scanning tunneling microscopy, Dirac bands, flat bands, chirality

INTRODUCTION

The honeycomb lattice, one of the three strongly isotropic lattices (honeycomb, diamond, and K_4 lattices [1-4]) is central to the modern two-dimensional (2D) materials because of its structural robustness and unique electronic properties [5-8]. In a tight-binding model where electrons can hop between nearest-neighbor nodes of the honeycomb lattice, linearly intersecting bands (Dirac bands) are formed near the Fermi level at the $\overline{\mathrm{K}}$ and $\overline{\mathrm{K}}'$ points of the Brillouin zone. Low-energy electronic excitations around these points behave as massless Dirac fermions with exotic properties and the bands become topologically non-trivial by an external perturbation or spin-orbit coupling [5, 9-14]. If the middle points of the neighboring nodes are chosen as hopping sites, the honeycomb lattice is transformed into the kagome lattice by the graph theory [15, 16]. The kagome lattice has not only Dirac bands but also flat bands, where the kinetic energies of electrons are quenched and electron correlation effects are strongly enhanced [17-19].

These Dirac and flat bands are under intensive investigations because of rich topological and/or many-body phenomena [20-24], but most of them are based on naturally grown inorganic materials and thus lack controllability of model parameters. One of the promising methods for extending the research realm is the usage of molecular assembly such as supramolecules [25-36] and metal-organic/covalent-organic frameworks [37-42], where 2D electronic lattices are defined by intermolecular networks [35, 39-41] or localized Schockley surface states coupled through molecular potential barriers [33, 34, 36]. This approach is based on rational design of molecules and thus can be very flexible and powerful. However, intermolecular coupling is often very weak and the general strategy for the formation of a molecular-based honeycomb lattice has not been established yet.

Here we adopt a non-planar π-conjugated molecule Trip-Phz (Fig. 1a) [43], a phenazine analog of triptycene, as a building block for fabricating 2D supramolecular assemblies with pristine molecular electronic bands (Fig.1b). Trip-Phz and related triptycene molecules are characterized by three polyhedral π-conjugated planes that create a rigid paddle-wheel shape with C_3-symmetry, and are known to form honeycomb supramolecular structures owing to their molecular symmetry [43-49]. Electronically, the assembled system can be viewed as a hybrid of the honeycomb and kagome lattices [36, 50-54]. Dirac and flat bands are predicted by a simple tight-binding model [46, 51, 55], but the validity of such an approach is not clear yet. This is particularly true when 2D molecular lattices are formed on a supporting substrate, which could strongly modify the intrinsic molecular states due to a finite interfacial interaction.

In this study, we successfully grow a purely 2D supramolecule of Trip-Phz on a Ag(111) substrate and elucidate its intriguing band structure. Our scanning tunneling microscopy (STM) observations reveal that Trip-Phz molecules form highly ordered honeycomb lattice that are both chiral and commensurate with the Ag(111) surface. Dirac and flat bands predicted by a tight-binding model are reproduced by total density functional theory (DFT) calculations including the Ag(111) substrate. This means that intrinsic molecular bands are protected from the substrate, which can be attributed to the unique geometry of the π-conjugated molecule. The present work

offers a general route for realizing pristine Dirac and flat bands through supramolecular assembly technique.

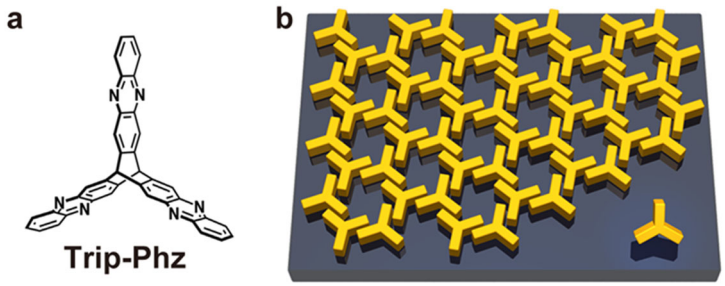

Figure 1. Molecular structure and formation of a honeycomb lattice. (a) Molecular structure of Trip-Phz. (b) Schematic illustration of a honeycomb lattice on a substrate.

RESULTS AND DISCUSSION

All experiments were carried out in UHV chambers with the base pressure less than 2.0×10^{-10} Torr (see Methods). Figure 2a shows an STM image of a Ag(111) surface partially covered with Trip-Phz molecules. In the right side of the image, a densely packed molecular lattice extends to an area of ~100 × 200 nm^2. The magnified STM image (Inset) shows that it indeed consists of honeycomb lattices as anticipated. A close inspection of the overall area reveals that the lattice includes only a small density of defects and no domain walls, signaling the formation of a 2D single crystal. The bright spots observed in the image are due to Trip-Phz molecules adsorbed on the lattice. Figure 2b shows another single-domain honeycomb lattice with a hole exposing a Ag surface. The height profile taken along the red line indicates a layer height of 0.3-0.4 nm, which is consistent with the standing configuration of phenazine moieties (the term "standing configuration" refers to the geometry where the π-conjugated planes of the molecule are placed in the surface normal direction). However, other molecular structures were routinely observed and the honeycomb lattice was found to cover only ~5% of the whole surface, suggesting that it is not energetically most stable. Most of coexisting phases are meandering ribbon-like structures when the coverage is small, as seen in the left side of Fig. 2a. When the coverage is increased, the molecule tends to form periodic 2D patterns that are distinct from the honeycomb lattice (Supporting Information, Fig. S1a-c). They seem to be stabilized by a configuration where two of the three π-conjugated planes of the molecule face toward the substrate surface, but its details are not clear at this stage. These structures were not transformed into a honeycomb lattice even by a post annealing. We note that similar non-honeycomb lattices were formed when a related triptycene derivative was directly deposited on a graphite or Au(111) surface [47, 49]. In this case, surface passivation with alkane molecules or iodine led to the formation of the honeycomb lattice,

respectively.

One way to overcome this problem without surface passivation is to dope alkali metals. Figure 2c displays an STM image of Trip-Phz molecules on a Ag(111) substrate that was co-

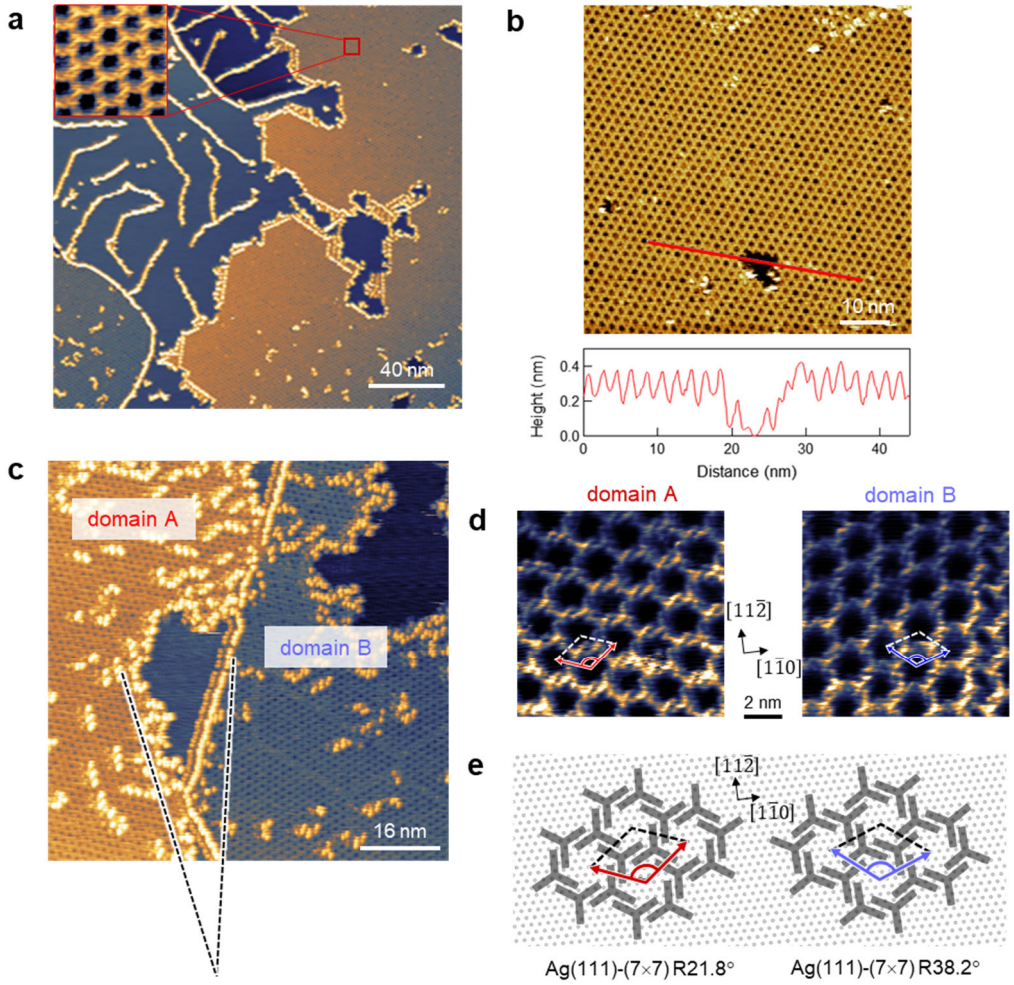

Figure 2. Honeycomb lattices of Trip-Phz supramolecule. (a) STM image of Trip-Phz molecules adsorbed on a Ag(111) surface (Sample bias voltage : V_s = -2 V, Tunneling current : I_t = 8.9 pA). Inset: high-resolution STM image corresponding to the red square region(Size: 8 nm ×8 nm, V_s = -2 V, I_t = 100 pA). (b) STM image of Trip-Phz molecules and the height profile taken along the red line. (c) STM image of Trip-Phz molecules adsorbed on a Ag(111) surface that was co-deposited with ~0.01 ML Cs and annealed at ~100 °C (V_s = -2 V, I_t = 10 pA). Domains A and B have different lattice orientations as indicated by the dashed lines. (d) High resolution STM images of domains A and B (constant height mode, size: 10 nm × 10 nm, V_s = -2 V. The feedback was stabilized at I_t = 10 pA). The arrows on the images indicate the unit vectors of honeycomb lattices, while those between the images the crystal orientations of the Ag(111) surface. (e) Structure model of Trip-Phz adsorbed on a Ag(111) surface. Left: Ag(111)-(7×7) R21.8°, Right: Ag(111)- (7×7) R38.2°. The arrows correspond to those in d.

deposited with ~0.01 ML Cs and annealed at ~370 K. By this treatment, the surface was preferentially covered by honeycomb lattices (Supporting Information, Fig. S1d, e). We did not find any deviation in structural parameters between non-doped and Cs-doped cases within the experimental accuracy. The doped Cs atoms should be located within the honeycomb pores, but are not visible because of the inaccessibility of the STM tip into deep holes (see the STM images of Fig. 2d below). Concerning the mechanism of lattice formation, Cs atoms could donate electrons to Trip-Phz and strengthen the π–π bonding between the neighboring moieties. This should lead to a shorter distance between them, but we did not observe a clear change experimentally (Supporting Information, Fig. S2). Rather, the Cs atoms may simply work as nucleation centers for crystal growth. We note that, even without Cs doping, electrons should be transferred from the Ag substrate to Trip-Phz and strengthens the bonding to some degree.

The honeycomb lattice of Trip-Phz molecules is chiral as a result of two possible stacking sequences of the π–π pancake bondings between moieties. Namely, while individual Trip-Phz molecules are achiral, they can acquire chirality by the formation of a supramolecule. Figure 2d shows high-resolution STM images with different chiralities, which were taken at domains A and B in Fig. 2c, respectively (see also Supporting Information, Fig. S3). They also have different lattice orientation as revealed by the unit vectors (also see the dashed lines in Fig. 2c). Interestingly, we find that all observed honeycomb lattices of the same chirality have the identical lattice orientation. This fact strongly indicates that the molecular adsorption geometry is well-defined and commensurate with the substrate surface. To determine the adsorption geometry, we quantified the lattice parameters precisely through careful calibrations and drift compensations. The lattice constant is found to be 1.99±0.04 nm, while the principal axes of the two chiral domains make an angle of 16.9 ±1.3°. The only superstructures of Trip-Phz compatible with these parameters are Ag(111)-(7×7) R21.8°/R38.2°, which give a lattice constant $7a_0 = 2.023$ nm ($a_0 = 0.289$ nm: the lattice constant of the Ag(111) surface) and the angle between principal axes 16.4° (= 38.2° − 21.8°). Mathematically, they are given by the matrices

$$\begin{pmatrix} 8 & 3 \\ -3 & 5 \end{pmatrix}, \quad \begin{pmatrix} 8 & 5 \\ -5 & 3 \end{pmatrix},$$

which represent the conversion between the unit vectors of the the Ag(111) and those of Trip-Phz lattices. Figure 2e shows schematic models of Ag(111)-(7×7) R21.8°/R38.2° superstructures. For both structures, the moieties are aligned along the $[11\bar{2}]$ and equivalent directions of Ag(111), which should stabilize these adsorption geometries. We note that, while the presence of a chiral honeycomb lattice was theoretically suggested [48], we directly show it here through STM observations.

In the following, we consider the electronic band structures of the Trip-Phz honeycomb lattice, first in the absence of the substrate. Trip-Phz consists of three phenazine moieties where the π-electrons form the lowest unoccupied molecular orbital (LUMO) and the highest occupied molecular orbital (HOMO). In an isolated Trip-Phz molecule, the LUMOs of the three moieties

forms two LUMOs and one LUMO+1 by intramolecular coupling (transfer integral) t_0. Similarly, the HOMOs of the three moieties form one HOMO and two HOMO-1 orbitals (Supporting Information, Fig. S5). In the honeycomb lattice with two independent sites in the unit cell, these LUMOs and HOMOs form six electronic bands separately through intermolecular coupling t_1. In a tight-binding model, the band structure is solely determined by the parameters t_0 and t_1 (Fig. 3a). Electronically, the present lattice can be viewed as a hybrid of honeycomb and kagome lattices. While this lattice model has been called star lattice or diatomic kagome lattice [36, 50-53], we refer to it as honeycomb-kagome lattice [54] to stress its hybrid character. In the two limiting cases of $t_0/t_1 \to \infty$ and $t_0/t_1 \to 0$, it corresponds to the pure honeycomb and kagome lattices, respectively (Fig. 3b).

Figure 3c shows the band diagrams calculated for three different values of t_0/t_1. For all cases, there exist two sets of Dirac bands linearly intersecting at $\bar{\mathrm{K}}$ point and two flat bands toughing the Dirac bands at $\bar{\Gamma}$ point. The flat bands here have the same origin as that of the kagome lattice; they arise due to a destructive interference from the neighboring sites and a resulting electron localization into the unit cell [17, 55]. Nevertheless, the band diagrams exhibit unique topologies different from that of a pure kagome lattice. For $t_0/t_1 > 2/3$ (left panel), the upper Dirac bands are isolated while the lower Dirac bands touch the two flat bands. With

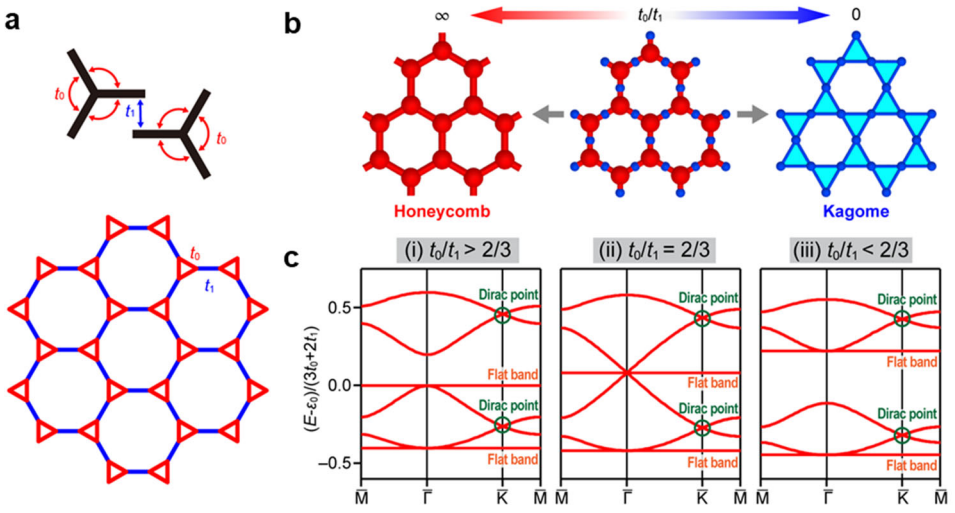

Figure 3. Tight-binding model of a honeycomb-kagome lattice. (a) Schematic illustration of intramolecular coupling t_0 and intermolecular coupling t_1(top) and honeycomb-kagome lattice (bottom). (b) Schematic illustration of the transition between the honeycomb lattice and the kagome lattice. $t_0/t_1 \to \infty$ and $t_0/t_1 \to 0$ correspond to the pure honeycomb and kagome lattices, respectively. (c) Band structures of honeycomb-kagome lattices along the high-symmetry $\bar{\mathrm{M}} - \bar{\Gamma} - \bar{\mathrm{K}} - \bar{\mathrm{M}}$ line: $t_0/t_1 > 2/3$ (left panel), $t_0/t_1 = 2/3$ (middle panel), $t_0/t_1 < 2/3$ (right panel).

decreasing t_0/t_1, the energy gap between the upper and lower Dirac bands decreases to zero and becomes "inverted" for $t_0/t_1 < 2/3$ (right panel). This results in two sets of kagome-like bands [51].

In the presence of the Ag substrate, these characteristic bands could strongly be modified or even disappear because of the interfacial interaction [56]. This motivates us to perform DFT calculations for the total system. The detailed adsorption geometry was determined by minimizing

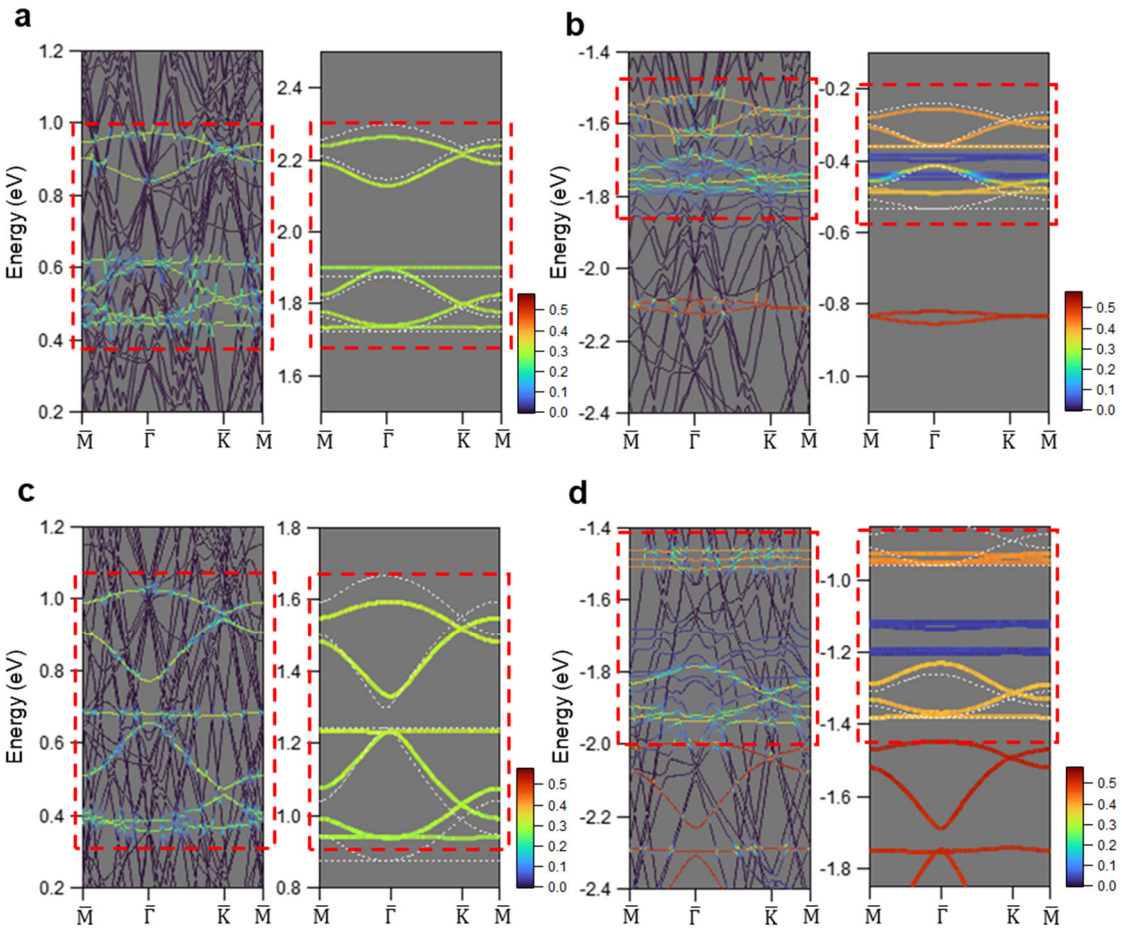

Figure 4. Theoretical calculations of band structures of the Trip-Phz honeycomb lattice on Ag(111). (a) Unoccupied states of Ag(111)-(7×7) R21.8°. (b) Occupied states of Ag(111)-(7×7) R21.8°. (c) Unoccupied states of hypothetical Ag(111)-(√43×√43). (d) Occupied states of hypothetical Ag(111)-(√43×√43). Left panels: Total DFT calculations. Right panels: DFT calculations without the Ag substrate (colored solid lines) and tight binding calculations with intramolecular coupling t_0 and intermolecular coupling t_1, which are deduced from the optimized structure (white dotted lines). The color scale represents the contribution of molecular π-orbitals to the density of states. The band structures indicated by the red dashed squares are LUMO and HOMO bands.

the total energy while maintaining the experimentally determined Ag(111)-(7×7) R21.8° superstructure (see Methods). The left panels of Fig. 4a, b show the calculated band structures along the high-symmetry $\bar{M}-\bar{\Gamma}-\bar{K}-\bar{M}$ line for the unoccupied states (0.2 eV < E < 1.2 eV) and occupied states (-2.4 eV < E < -1.4 eV). The molecule-derived bands can be identified by their bright colors that represents the contribution of π-orbitals to the density of states. They hardly intermix with Ag-derived bands represented by dark colors, suggesting a weak coupling between them. To investigate the influence of the substrate, we also calculated the band structures of free-standing molecules while keeping the optimized molecular structure. The right panels of Fig. 4a,b show the results for unoccupied states (1.5 eV < E < 2.5 eV) and occupied states (-1.1 eV < E < -0.1 eV). They are essentially the same as those of total calculations except for a constant energy shift, demonstrating the minor effects of the substrate.

The bands indicated by the dashed red squares in Fig. 4a, b are derived from LUMOs and HOMOs of Trip-Phz. To confirm the validity of the honeycomb-kagome lattice model of Fig. 3a, we show the results of the tight binding calculations as the white dotted lines in the right panels of Fig. 4a, b. Here the transfer integrals $t_0 =$ -0.141 eV and $t_1 =$ -0.076 eV (LUMO bands) and $t_0 = -0.040$ eV and $t_1 = -0.087$ eV (HOMO bands) were obtained from the energy splitting of a pair of phenazine moieties (see Methods). The semi-quantitative agreement with the DFT results demonstrates that the present molecular system is an ideal realization of the honeycomb-kagome lattice model. We note that the band topology expected for the LUMOs ($t_0/t_1 = 1.86 > 2/3$) and that for the HOMOs ($t_0/t_1 = 0.46 < 2/3$) are in agreement with those in Fig. 3d.

Here we examine the interaction between the molecules and the Ag substrate. As is widely known, π-conjugated molecules such as pentacene and phthalocyanine are adsorbed on a metal surface in a planar configuration, and their π-orbitals couples with the electrons in the substrate because of face-to-face configurations [26, 27, 29, 31, 33]. By contrast, Trip-Phz should be only weakly coupled with the substrate because their π-conjugated planes are set perpendicular to the surface. This effect is further strengthened by the presence of the C-H bondings; since they stick out in the normal direction, they lift up the π-orbitals in the moieties and weakens their coupling with the Ag surface. Thus, the molecular states can be protected by the unique adsorption geometry. Nevertheless, judging from the commensurability of lattices, the Ag(111) substrate must significantly influence the adsorption structure. These ideas are reinforced by calculating the spatial distribution of differential charge induced by the molecular adsorption (Supporting Information, Fig. S6); differential charge is nearly absent on the π-orbitals of the moieties, while it is concentrated on the σ-orbitals of C, H, N atoms at the interface. The importance of the interfacial interaction is also suggested by the fact that the Trip-Phz honeycomb lattice is not stabilized in the DFT calculations in the absence of the Ag(111) substrate.

The above theoretical results can be compared to our scanning tunneling spectroscopy (STS) measurements. Figure 5 shows a *dI/dV* spectrum taken on Trip-Phz molecules on Ag(111) (red

solid line). The spectrum is the average over an about 2.5 nm × 2.5 nm area, which is larger than the unit cell of the honeycomb lattice. Within this region, we did not observe a noticeable site dependence of spectra (see Supporting Information, Fig. S4). Clear peaks around -1.3 V and -1.6 V correspond to the HOMO bands in Fig. 4b, while the weak peak structures around +0.5 V and +0.8 V (designated by the solid arrows) originate from the LUMO bands in Fig. 4a. The peak around +0.2 eV (designated by the dotted arrow) is attributed to the onset of the Ag(111) surface states, which is likely to be shifted due to the presence of molecules (for the spectrum on a clean Ag(111) surface, see the blue solid line) [57]. The strong disparity of the signal intensities of the HOMO and LUMO bands may be attributed to the existence of wavefunction nodes and phase inversions along the phenazine moieties (Supporting Information, Fig. S5). Supposing that the wavefunction of the STM tip apex consists of an *s*-orbital, the amplitude of electron tunneling between the tip apex to the LUMO bands could be suppressed because of destructive interferences among neighboring tip-molecule paths. By contrast, the number of nodes in the wavefunctions is smaller for the HOMO bands (i.e., the nodes are more separated), making this mechanism less effective. We also note that the Ag *d*-bands are present in the occupied side, which give a high density of states. This will elevate the base line for HOMO band peaks and make them apparently higher. It can also increase the electron transfer from the molecules to the STM tip, thus leading to a real enhancement of the spectral peaks.

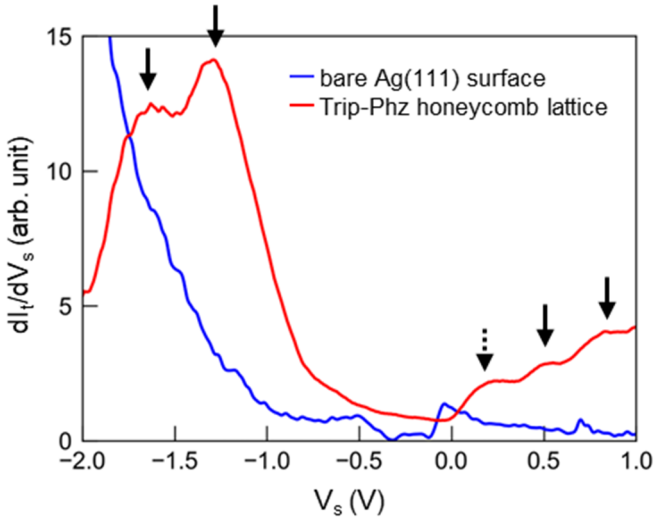

Figure 5. *dI/dV* spectrum taken on Trip-Phz molecules on Ag(111) (red solid curve). I_t –V_s curves were obtained at a constant height after the feedback was stabilized at V_s = -2 V, I_t = 10 pA. The data were numerically differentiated and were averaged over about a 2.5 nm × 2.5 nm area to obtain the spectrum. As a control measurement, *dI/dV* spectrum was also taken on a clean Ag(111) surface (blue solid line). It was directly obtained using the lock-in technique (modulation amplitude : 10 mV, frequency : 743 Hz) at a constant height. The feedback was stabilized at V_s = -2 V, I_t = 100 pA.

We did not observe fine spectroscopic features corresponding to the flat and Dirac bands obtained by the DFT calculations. This is reasonable considering the relatively narrow band widths of ~0.2 eV in our system, which is much smaller than that of ~10 eV of graphene. The molecular levels of a large organic molecule are commonly detected as broad features in STS. This is true even if the molecule is decoupled from the metallic substrate by a thin insulating layer and the intrinsic molecular levels remain sufficiently sharp [58, 59]. This apparent level broadening in STS measurement is likely to be caused by the presence of many energy relaxation paths for an electronically excited large organic molecule. Nevertheless, the unique band structures predicted here can strongly influence the electron transport properties at low temperatures, where the physics is governed by the low-energy electrons.

Finally, we note that the widths of the Dirac bands are sensitive to the periodicity of the molecular superlattice. To see this effect, we calculated using the same methods the band structures of a hypothetical Ag(111)-(√43×√43) superstructure, for which the unit length is reduced by 6.3% from that of Ag(111)-(7×7) R21.8°. In Fig. 4c, d, the results are shown in the same manner as in Fig. 4a, b (left panels: total DFT calculations, right panels: DFT calculations without the substrate and tight binding calculations). For the LUMO bands, the widths of the Dirac bands are significantly enhanced compared to those of the Ag(111)-(7×7) R21.8°. This conspicuous change is attributed to a variation in intermolecular coupling t_1; we obtained $t_1 =$ -0.185 eV for the LUMO bands of Ag(111)-(√43×√43), which is 2.4 times the t_1 value for Ag(111)-(7×7) R21.8°. As mentioned above, the orbitals of the phenazine moiety has several nodes along the plane. Therefore, a small shift in the geometry can significantly change the behavior of interference between neighboring orbitals. This suggests the tunability of the Dirac bands using an external perturbation. For example, a simple replacement of Ag(111) by another surface with a different lattice constant may strongly modify the Dirac band widths.

CONCLUSIONS

In summary, we have successfully observed using STM that Trip-Phz molecules form chiral and commensurate honeycomb lattices on a Ag(111) surface. The tight-binding and DFT calculations reveal that the present molecular system is an ideal realization of the honeycomb-kagome lattice model. Notably, intrinsic electronic bands are protected from the supporting metal surface due to the non-planar adsorption geometry of Trip-Phz molecules. It is also worth noting that the molecular assembly acquires chirality as a result of stacking sequences of the π–π pancake bondings, which is another consequence of using non-planar π conjugated molecule. This "emergent" chirality may play important roles in spin-related phenomena and optical sensitivity [60]. The present work offers a general strategy for fabricating chiral supramolecules that can accommodate pristine Dirac and flat bands simultaneously.

METHODS

Preparation and purification of Trip-Phz

The triptycene derivative Trip-Phz was prepared according to the procedure described in the literature [43] and purified by sublimation at 450 K under a reduced pressure of 10^{-2} mbar.

Sample preparation and STM measurements

Sample preparations and STM measurements were performed under UHV environment (< 2.0×10^{-10} mbar). A Ag(111) single crystal (MaTecK, 99.999%) was used as a substrate. The substrate surface was cleaned to achieve atomically flat surfaces by subjecting it to multiple cycles of Ar^+ sputtering and annealing (~700 K) processes. After cleaning the Ag(111) surface, Trip-Phz was deposited using a homebuilt molecular evaporator (thermal radiation heating). Cs was deposited using an alkali metal dispenser (SAES, CS/NF/3.9/12 FT10+10). Prior to each process, the deposition rate was monitored using a quartz crystal microbalance.

STM measurements were carried out with Ar^+-sputtered Pt-Ir tip at 4.6 K. All STM images were taken in constant current mode except for Fig. 2d. To precisely determine the honeycomb lattice parameters, the coefficients of the piezo scanner tube were calibrated by referring to atomic images of Ag(111). The lateral drift during the acquisition of an STM image were compensated by assuming a constant drift speed. The STS data were acquired at 32 locations and averaged. Before the measurement, *dI/dV* spectra were taken on a clean Ag(111) surface. The observation of the surface states, which exhibit themselves as a step-like feature at $V \sim$ -70 mV [57], ensures the cleanliness of the STM tip.

DFT calculations

DFT calculations were conducted using the Vienna Ab initio Simulation Package (VASP) [61, 62] with the projected augmented wave (PAW) potentials [63] and the generalized gradient approximation (GGA). The exchange-correlation functional employed was Perdew-Burke-Ernzerhof (PBE) [64], incorporating nonlocal van der Waals interaction (rev-vdW-DF2) [65]. The plane-wave basis set energy cutoff was set at 400 eV. The modeling of Trip-Phz on Ag(111) involved using a supercell consisting of two Trip-Phz molecules on a three-layer Ag(111)-(7×7) slab, with a vacuum thickness of approximately 16 Å along the surface normal. To determine the equilibrium crystal structures, a conjugate-gradient relaxation of ionic positions was performed until the Hellmann-Feynman force on each atom was less than 0.02 eV/Å, with the exception of the bottom Ag layer. The atoms in the bottom layer were held at their ideal bulk positions during the structure optimization. For the self-consistent total energy calculations, the Brillouin zone was sampled using Monkhorst–Pack grids [66] with 9 × 9 × 1 k-points.

To determine the intramolecular coupling t_0 and the intermolecular coupling t_1, we used the Gaussian 16 program package [67]. We set isolated pairs of phenazine moieties corresponding to the intra/inter-molecular coupling, the atomic coordinates of which were taken from the results

of the VASP DFT calculations. The calculated level splittings of the pairs were identified with t_0 and t_1.

ASSOCIATED CONTENT

Supporting Information

The Supporting Information is available online. It includes the following contents: STM images of Trip-Phz layers on a Ag(111) surface grown under various conditions (Fig. S1), comparison of the distances between neighboring phenazine moieties in the Trip-Phz honeycomb lattice before and after Cs deposition (Fig. S2), STM images of Trip-Phz honeycomb lattices on a Ag(111) surface processed for a clearer view (Fig. S3), the site dependence of the dI/dV spectra of a Trip-Phz honeycomb lattice on a Ag(111) surface with Cs doping (Fig. S4), the energy levels and spatial distributions of LUMOs and HOMOs of the phenazine moiety and Trip-Phz (Fig. S5), and DFT-calculated spatial distributions of differential charge for a Trip-Phz honeycomb lattice on a Ag(111) surface (Fig. S6).

AUTHOR INFORMATION

Corresponding Authors

Rie Suizu — Department of Chemistry and IRCCS, Nagoya University, Furo-cho, Chikusa-ku, Nagoya 464-8602, Japan; Email: suizu@chem.nagoya-u.ac.jp

Takashi Uchihashi — Research Centre for Materials Nanoarchitectonics (MANA), National Institute for Materials Science, 1-1, Namiki, Tsukuba, Ibaraki 305-0044, Japan; Email: UCHIHASHI.Takashi@nims.go.jp

Kunio Awaga — Department of Chemistry and IRCCS, Nagoya University, Furo-cho, Chikusa-ku, Nagoya 464-8602, Japan; Email: awaga.kunio.h8@f.mail.nagoya-u.ac.jp

Authors

Ryohei Nemoto — Research Center for Materials Nanoarchitectonics (MANA), National Institute for Materials Science, 1-1, Namiki, Tsukuba, Ibaraki 305-0044, Japan

Ryuichi Arafune — Research Center for Materials Nanoarchitectonics (MANA), National Institute for Materials Science, 1-1, Namiki, Tsukuba, Ibaraki 305-0044, Japan

Saya Nakano — Department of Physics, Nara Women's University, Kitauoyanishi-machi, Nara 630-8506, Japan

Masahisa Tsuchiizu — Department of Physics, Nara Women's University, Kitauoyanishi-machi, Nara 630-8506, Japan

Noriaki Takagi — Graduate School of Human and Environmental Studies, Kyoto Univeristy, Yoshida-nihonmatsu-cho, Sakyo-ku, Kyoto 606-8501, Japan

Author Contributions

The manuscript was written through contributions of all authors. All authors have given approval to the final version of the manuscript.

Notes

The authors declare no competing financial interest.

ACKNOWLEDGMENTS

The authors thank T. Nakamura for his technical supports for the STM experiments. This work was supported financially by JSPS KAKENHI (Grant Numbers 20H05621, 20H02707, 22H0196), Japan Science and Technology Agency (JST) PRESTO Grant JPMJPR21A9, and World Premier International Research Center (WPI) Initiative on Materials Nanoarchitectonics, MEXT, Japan.

REFERENCES

(1) Sunda, T. *Topological Crystallography With a View Towards Discrete Geometric Analysis*; Springer, 2013.

(2) Itoh, M.; Kotani, M.; Naito, H.; Sunada, T.; Kawazoe, Y.; Adschiri, T. New Metallic Carbon Crystal. *Phys. Rev. Lett.* **2009**, *102*, 055703.

(3) Mizuno, A.; Shuku, Y.; Suizu, R.; Matsushita, M. M.; Tsuchiizu, M.; Reta Maneru, D.; Illas, F.; Robert, V.; Awaga, K. Discovery of the K4 Structure Formed by a Triangular π Radical Anion. *J. Am. Chem. Soc.* **2015**, *137*, 7612-7615.

(4) Tsuchiizu, M. Three-dimensional higher-spin Dirac and Weyl dispersions in the strongly isotropic K4 crystal. *Phys. Rev. B* **2016**, *94*, 195426.

(5) Novoselov, K. S.; Geim, A. K.; Morozov, S. V.; Jiang, D.; Katsnelson, M. I.; Grigorieva, I. V.; Dubonos, S. V.; Firsov, A. A. Two-dimensional gas of massless Dirac fermions in graphene. *Nature* **2005**, *438*, 197-200.

(6) Vogt, P.; De Padova, P.; Quaresima, C.; Avila, J.; Frantzeskakis, E.; Asensio, M.; Resta, A.; Ealet, B.; Le Lay, G. Silicene: Compelling Experimental Evidence for Graphenelike Two-Dimensional Silicon. *Phys. Rev. Lett.* **2012**, *108*, 155501.

(7) Tang, Q.; Zhou, Z. Graphene-analogous low-dimensional materials. *Prog. Mater. Sci.* **2013**, *58*, 1244-1315.

(8) Reis, F.; Li, G.; Dudy, L.; Bauernfeind, M.; Glass, S.; Hanke, W.; Thomale, R.; Schäfer, J.; Claessen, R. Bismuthene on a SiC substrate: A candidate for a high-temperature quantum spin Hall material. *Science* **2017**, *357*, 287-290.

(9) Ando, T.; Nakanishi, T.; Saito, R. Berry's Phase and Absence of Back Scattering in Carbon Nanotubes. *J. Phys. Soc. Jpn.* **1998**, *67*, 2857-2862.

(10) Haldane, F. D. M. Model for a Quantum Hall Effect without Landau Levels: Condensed-Matter Realization of the "Parity Anomaly". *Phys. Rev. Lett.* **1988**, *61*, 2015-2018.

(11) Kane, C. L.; Mele, E. J. Z_{2} Topological Order and the Quantum Spin Hall Effect. *Phys. Rev. Lett.* **2005**, *95*, 146802.

(12) Klimovskikh, I. I.; Otrokov, M. M.; Voroshnin, V. Y.; Sostina, D.; Petaccia, L.; Di Santo, G.; Thakur, S.; Chulkov, E. V.; Shikin, A. M. Spin–Orbit Coupling Induced Gap in Graphene on Pt(111) with Intercalated Pb Monolayer. *ACS Nano* **2017**, *11*, 368-374.

(13) McIver, J. W.; Schulte, B.; Stein, F. U.; Matsuyama, T.; Jotzu, G.; Meier, G.; Cavalleri, A. Light-induced anomalous Hall effect in graphene. *Nat. Phys.* **2020**, *16*, 38-41.

(14) Liu, C.-C.; Feng, W.; Yao, Y. Quantum Spin Hall Effect in Silicene and Two-Dimensional Germanium. *Phys. Rev. Lett.* **2011**, *107*, 076802.

(15) Zhou, M.; Liu, Z.; Ming, W.; Wang, Z.; Liu, F. sd2 Graphene: Kagome Band in a Hexagonal Lattice. *Phys. Rev. Lett.* **2014**, *113*, 236802.

(16) Suizu, R.; Awaga, K. Line graph theory reveals hidden spin frustration and bond frustration in molecular crystals with strong isotropy. *J. Mater. Chem. C* **2022**, *10*, 1196-1203.
(17) Guo, H. M.; Franz, M. Topological insulator on the kagome lattice. *Phys. Rev. B* **2009**, *80*, 113102.
(18) Tang, E.; Mei, J.-W.; Wen, X.-G. High-Temperature Fractional Quantum Hall States. *Phys. Rev. Lett.* **2011**, *106*, 236802.
(19) BERGHOLTZ, E. J.; LIU, Z. Topological Flat Band Models And Fractional Chern Insulators. *Int. J. Mod. Phys. B* **2013**, *27*, 1330017.
(20) Lin, Z.; Choi, J.-H.; Zhang, Q.; Qin, W.; Yi, S.; Wang, P.; Li, L.; Wang, Y.; Zhang, H.; Sun, Z.; Wei, L.; Zhang, S.; Guo, T.; Lu, Q.; Cho, J.-H.; Zeng, C.; Zhang, Z. Flatbands and Emergent Ferromagnetic Ordering in Fe3Sn2 Kagome Lattices. *Phys. Rev. Lett.* **2018**, *121*, 096401.
(21) Ye, L.; Kang, M.; Liu, J.; von Cube, F.; Wicker, C. R.; Suzuki, T.; Jozwiak, C.; Bostwick, A.; Rotenberg, E.; Bell, D. C.; Fu, L.; Comin, R.; Checkelsky, J. G. Massive Dirac fermions in a ferromagnetic kagome metal. *Nature* **2018**, *555*, 638-642.
(22) Kang, M.; Ye, L.; Fang, S.; You, J.-S.; Levitan, A.; Han, M.; Facio, J. I.; Jozwiak, C.; Bostwick, A.; Rotenberg, E.; Chan, M. K.; McDonald, R. D.; Graf, D.; Kaznatcheev, K.; Vescovo, E.; Bell, D. C.; Kaxiras, E.; van den Brink, J.; Richter, M.; Prasad Ghimire, M.; Checkelsky, J. G.; Comin, R. Dirac fermions and flat bands in the ideal kagome metal FeSn. *Nat. Mat.* **2020**, *19*, 163-169.
(23) Sun, Z.; Zhou, H.; Wang, C.; Kumar, S.; Geng, D.; Yue, S.; Han, X.; Haraguchi, Y.; Shimada, K.; Cheng, P.; Chen, L.; Shi, Y.; Wu, K.; Meng, S.; Feng, B. Observation of Topological Flat Bands in the Kagome Semiconductor Nb3Cl8. *Nano Lett.* **2022**, *22*, 4596-4602.
(24) Yin, J.-X.; Lian, B.; Hasan, M. Z. Topological kagome magnets and superconductors. *Nature* **2022**, *612*, 647-657.
(25) Wang, Q. H.; Hersam, M. C. Room-temperature molecular-resolution characterization of self-assembled organic monolayers on epitaxial graphene. *Nat. Chem.* **2009**, *1*, 206-211.
(26) Shi, Z.; Lin, N. Porphyrin-Based Two-Dimensional Coordination Kagome Lattice Self-Assembled on a Au(111) Surface. *J. Am. Chem. Soc.* **2009**, *131*, 5376-5377.
(27) Mao, J.; Zhang, H.; Jiang, Y.; Pan, Y.; Gao, M.; Xiao, W.; Gao, H. J. Tunability of Supramolecular Kagome Lattices of Magnetic Phthalocyanines Using Graphene-Based Moiré Patterns as Templates. *J. Am. Chem. Soc.* **2009**, *131*, 14136-14137.
(28) Wang, Y.; Ge, X.; Manzano, C.; Kröger, J.; Berndt, R.; Hofer, W. A.; Tang, H.; Cerda, J. Supramolecular Patterns Controlled by Electron Interference and Direct Intermolecular Interactions. *J. Am. Chem. Soc.* **2009**, *131*, 10400-10402.
(29) Tanaka, Y.; Mishra, P.; Tateishi, R.; Cuong, N. T.; Orita, H.; Otani, M.; Nakayama, T.; Uchihashi, T.; Sakamoto, K. Highly Ordered Cobalt Phthalocyanine Chains on Fractional Atomic

Steps: One-Dimensionality and Electron Hybridization. *Acs Nano* **2013**, *7*, 1317–1323.
(30) Yamamoto, M.; Suizu, R.; Dutta, S.; Mishra, P.; Nakayama, T.; Sakamoto, K.; Wakabayashi, K.; Uchihashi, T.; Awaga, K. Self-assembled honeycomb lattice in the monolayer of cyclic thiazyl diradical BDTDA (= 4,4′-bis(1,2,3,5-dithiadiazolyl)) on Cu(111) with a zero-bias tunneling spectra anomaly. *Sci. Rep.* **2015**, *5*, 18359.
(31) Yoshizawa, S.; Minamitani, E.; Vijayaraghavan, S.; Mishra, P.; Takagi, Y.; Yokoyama, T.; Oba, H.; Nitta, J.; Sakamoto, K.; Watanabe, S.; Nakayama, T.; Uchihashi, T. Controlled Modification of Superconductivity in Epitaxial Atomic Layer–Organic Molecule Heterostructures. *Nano Lett.* **2017**, *17*, 2287-2293.
(32) Kaposi, T.; Joshi, S.; Hoh, T.; Wiengarten, A.; Seufert, K.; Paszkiewicz, M.; Klappenberger, F.; Ecija, D.; Đorđević, L.; Marangoni, T.; Bonifazi, D.; Barth, J. V.; Auwärter, W. Supramolecular Spangling, Crocheting, and Knitting of Functionalized Pyrene Molecules on a Silver Surface. *ACS Nano* **2016**, *10*, 7665-7674.
(33) Lobo-Checa, J.; Matena, M.; Muller, K.; Dil, J. H.; Meier, F.; Gade, L. H.; Jung, T. A.; Stohr, M. Band Formation from Coupled Quantum Dots Formed by a Nanoporous Network on a Copper Surface. *Science* **2009**, *325*, 300-303.
(34) Piquero-Zulaica, I.; Lobo-Checa, J.; Sadeghi, A.; El-Fattah, Z. M. A.; Mitsui, C.; Okamoto, T.; Pawlak, R.; Meier, T.; Arnau, A.; Ortega, J. E.; Takeya, J.; Goedecker, S.; Meyer, E.; Kawai, S. Precise engineering of quantum dot array coupling through their barrier widths. *Nat. Commun.* **2017**, *8*, 787.
(35) Pan, M.; Zhang, X.; Zhou, Y.; Wang, P.; Bian, Q.; Liu, H.; Wang, X.; Li, X.; Chen, A.; Lei, X.; Li, S.; Cheng, Z.; Shao, Z.; Ding, H.; Gao, J.; Li, F.; Liu, F. Growth of Mesoscale Ordered Two-Dimensional Hydrogen-Bond Organic Framework with the Observation of Flat Band. *Phys. Rev. Lett.* **2023**, *130*, 036203.
(36) Yin, R.; Zhu, X.; Fu, Q.; Hu, T.; Wan, L.; Wu, Y.; Liang, Y.; Wang, Z.; Qiu, Z.-L.; Tan, Y.-Z.; Ma, C.; Tan, S.; Hu, W.; Li, B.; Wang, Z. F.; Yang, J.; Wang, B. Artificial kagome lattices of Shockley surface states patterned by halogen hydrogen-bonded organic frameworks. *Nat. Commun.* **2024**, *15*, 2969.
(37) Wang, Z. F.; Liu, Z.; Liu, F. Organic topological insulators in organometallic lattices. *Nat. Commun.* **2013**, *4*, 1471.
(38) Yamada, M. G.; Soejima, T.; Tsuji, N.; Hirai, D.; Dincă, M.; Aoki, H. First-principles design of a half-filled flat band of the kagome lattice in two-dimensional metal-organic frameworks. *Phys. Rev. B* **2016**, *94*, 081102.
(39) Steiner, C.; Gebhardt, J.; Ammon, M.; Yang, Z.; Heidenreich, A.; Hammer, N.; Görling, A.; Kivala, M.; Maier, S. Hierarchical on-surface synthesis and electronic structure of carbonyl-functionalized one- and two-dimensional covalent nanoarchitectures. *Nat. Commun.* **2017**, *8*,

14765.
(40) Joshi, T.; Chen, C.; Li, H.; Diercks, C. S.; Wang, G.; Waller, P. J.; Li, H.; Bredas, J.-L.; Yaghi, O. M.; Crommie, M. F. Local Electronic Structure of Molecular Heterojunctions in a Single-Layer 2D Covalent Organic Framework. *Adv. Mater.* **2019**, *31*, 1805941.
(41) Rizzo, D. J.; Dai, Q.; Bronner, C.; Veber, G.; Smith, B. J.; Matsumoto, M.; Thomas, S.; Nguyen, G. D.; Forrester, P. R.; Zhao, W.; Jørgensen, J. H.; Dichtel, W. R.; Fischer, F. R.; Li, H.; Bredas, J.-L.; Crommie, M. F. Revealing the Local Electronic Structure of a Single-Layer Covalent Organic Framework through Electronic Decoupling. *Nano Lett.* **2020**, *20*, 963-970.
(42) Xiong, J.; Qin, T.; Hu, L.; Yang, W.; Chen, Z.; Ding, H.; Hu, J.; Xu, Q.; Zhu, J. On-Surface Synthesis of Novel Kagome Lattices Coordinated via Four-Fold N–Ag Bonding. *J. Phys. Chem. Lett.* **2023**, *14*, 9787-9792.
(43) Ushiroguchi, R.; Shuku, Y.; Suizu, R.; Awaga, K. Variable Host–Guest Charge-Transfer Interactions in 1D Channels Formed in a Molecule-Based Honeycomb Lattice of Phenazine Analogue of Triptycene. *Cryst. Growth Des.* **2020**, *20*, 7593-7597.
(44) Bhola, R.; Payamyar, P.; Murray, D. J.; Kumar, B.; Teator, A. J.; Schmidt, M. U.; Hammer, S. M.; Saha, A.; Sakamoto, J.; Schlüter, A. D.; King, B. T. A Two-Dimensional Polymer from the Anthracene Dimer and Triptycene Motifs. *J. Am. Chem. Soc.* **2013**, *135*, 14134-14141.
(45) Kissel, P.; Murray, D. J.; Wulftange, W. J.; Catalano, V. J.; King, B. T. A nanoporous two-dimensional polymer by single-crystal-to-single-crystal photopolymerization. *Nat. Chem.* **2014**, *6*, 774-778.
(46) Shuku, Y.; Mizuno, A.; Ushiroguchi, R.; Hyun, C. S.; Ryu, Y. J.; An, B. K.; Kwon, J. E.; Park, S. Y.; Tsuchiizu, M.; Awaga, K. An exotic band structure of a supramolecular honeycomb lattice formed by a pancake pi-pi interaction between triradical trianions of triptycene tribenzoquinone. *Chem. Commun.* **2018**, *54*, 3815-3818.
(47) Grossmann, L.; King, B. T.; Reichlmaier, S.; Hartmann, N.; Rosen, J.; Heckl, W. M.; Bjork, J.; Lackinger, M. On-surface photopolymerization of two-dimensional polymers ordered on the mesoscale. *Nat. Chem.* **2021**, *13*, 730-736.
(48) Das, S.; Nascimbeni, G.; de la Morena, R. O.; Ishiwari, F.; Shoji, Y.; Fukushima, T.; Buck, M.; Zojer, E.; Zharnikov, M. Porous Honeycomb Self-Assembled Monolayers: Tripodal Adsorption and Hidden Chirality of Carboxylate Anchored Triptycenes on Ag. *ACS Nano* **2021**, *15*, 11168-11179.
(49) Grossmann, L.; Ringel, E.; Rastgoo-Lahrood, A.; King, B. T.; Rosen, J.; Heckl, W. M.; Opris, D.; Björk, J.; Lackinger, M. Steering Self-Assembly of Three-Dimensional Iptycenes on Au(111) by Tuning Molecule-Surface Interactions. *Angew. Chem. Int.* **2022**, *61*, e202201044.
(50) Jiang, W.; Ni, X.; Liu, F. Exotic Topological Bands and Quantum States in Metal–Organic and Covalent–Organic Frameworks. *Acc. Chem. Res.* **2021**, *54*, 416-426.

(51) Mizoguchi, T.; Maruyama, M.; Okada, S.; Hatsugai, Y. Flat bands and higher-order topology in polymerized triptycene: Tight-binding analysis on decorated star lattices. *Phys. Rev. Mater.* **2019**, *3*, 114201.
(52) Springer, M. A.; Liu, T.-J.; Kuc, A.; Heine, T. Topological two-dimensional polymers. *Chem. Soc. Rev.* **2020**, *49*, 2007-2019.
(53) Zheng, Y.-Z.; Tong, M.-L.; Xue, W.; Zhang, W.-X.; Chen, X.-M.; Grandjean, F.; Long, G. J. A "Star" Antiferromagnet: A Polymeric Iron(III) Acetate That Exhibits Both Spin Frustration and Long-Range Magnetic Ordering. *Angew. Chem. Int.* **2007**, *46*, 6076-6080.
(54) Telychko, M.; Li, G.; Mutombo, P.; Soler-Polo, D.; Peng, X.; Su, J.; Song, S.; Koh, M. J.; Edmonds, M.; Jelínek, P.; Wu, J.; Lu, J. Ultrahigh-yield on-surface synthesis and assembly of circumcoronene into a chiral electronic Kagome-honeycomb lattice. *Sci. Adv.* **2021**, *7*, eabf0269.
(55) Shuku, Y.; Suizu, R.; Nakano, S.; Tsuchiizu, M.; Awaga, K. Engineering Dirac cones and topological flat bands with organic molecules. *Phys. Rev. B* **2023**, *107*, 155123.
(56) Lin, C.-L.; Arafune, R.; Kawahara, K.; Kanno, M.; Tsukahara, N.; Minamitani, E.; Kim, Y.; Kawai, M.; Takagi, N. Substrate-Induced Symmetry Breaking in Silicene. *Phys. Rev. Lett.* **2013**, *110*, 076801.
(57) Kliewer, J.; Berndt, R.; Chulkov, E. V.; Silkin, V. M.; Echenique, P. M.; Crampin, S. Dimensionality Effects in the Lifetime of Surface States. *Science* **2000**, *288*, 1399-1402.
(58) Kim, S. H.; Jeong, H. G.; Lim, S. J.; Ham, U. D.; Song, Y. J.; Yu, J.; Kuk, Y. Geometric and electronic properties of porphyrin molecules on Au(111) and NaCl surfaces. *Surf. Sci.* **2013**, *613*, 54-57.
(59) Imada, H.; Miwa, K.; Imai-Imada, M.; Kawahara, S.; Kimura, K.; Kim, Y. Real-space investigation of energy transfer in heterogeneous molecular dimers. *Nature* **2016**, *538*, 364-367.
(60) Göhler, B.; Hamelbeck, V.; Markus, T. Z.; Kettner, M.; Hanne, G. F.; Vager, Z.; Naaman, R.; Zacharias, H. Spin Selectivity in Electron Transmission Through Self-Assembled Monolayers of Double-Stranded DNA. *Science* **2011**, *331*, 894-897.
(61) Kresse, G.; Furthmüller, J. Efficient iterative schemes for ab initio total-energy calculations using a plane-wave basis set. *Phys. Rev. B* **1996**, *54*, 11169-11186.
(62) Kresse, G.; Furthmüller, J. Efficiency of ab-initio total energy calculations for metals and semiconductors using a plane-wave basis set. *Comput. Mater. Sci* **1996**, *6*, 15-50.
(63) Blöchl, P. E. Projector augmented-wave method. *Phys. Rev. B* **1994**, *50*, 17953-17979.
(64) Perdew, J. P.; Burke, K.; Ernzerhof, M. Generalized Gradient Approximation Made Simple. *Phys. Rev. Lett.* **1996**, *77*, 3865-3868.
(65) Hamada, I. van der Waals density functional made accurate. *Phys. Rev. B* **2014**, *89*, 121103.
(66) Monkhorst, H. J.; Pack, J. D. Special points for Brillouin-zone integrations. *Phys. Rev. B* **1976**, *13*, 5188-5192.

(67) Gaussian 16, Revision C.01. Gaussian, Inc., Wallingford CT, 2016.